Analytical potential for atomistic simulations of silicon, carbon, and silicon carbide

Paul Erhart* and Karsten Albe

Technische Universität Darmstadt, Institut für Materialwissenschaft, Petersenstr. 23, D-64287 Darmstadt, Germany
(Received 13 August 2004; published 19 January 2005)

We present an analytical bond-order potential for silicon, carbon, and silicon carbide that has been optimized by a systematic fitting scheme. The functional form is adopted from a preceding work [Phys. Rev. B **65**, 195124 (2002)] and is built on three independently fitted potentials for Si—Si, C—C, and Si—C interaction. For elemental silicon and carbon, the potential perfectly reproduces elastic properties and agrees very well with first-principles results for high-pressure phases. The formation enthalpies of point defects are reasonably reproduced. In the case of silicon stuctural features of the melt agree nicely with data taken from literature. For silicon carbide the dimer as well as the solid phases B1, B2, and B3 were considered. Again, elastic properties are very well reproduced including internal relaxations under shear. Comparison with first-principles data on point defect formation enthalpies shows fair agreement. The successful validation of the potentials for configurations ranging from the molecular to the bulk regime indicates the transferability of the potential model and makes it a good choice for atomistic simulations that sample a large configuration space.

I. INTRODUCTION

Silicon carbide is a compound semiconductor, which is of fundamental and technological interest, because of its electronic as well as mechanical properties.[1,2] It features extreme hardness, chemical resistivity, excellent mechanical properties at high-temperature, large thermal conductivity, and high-temperature semiconductivity.[3–6]

Over the last decades, atomistic computer simulations based on molecular dynamics (MD), molecular statics, or Monte Carlo (MC) methods have evolved as invaluable tools in condensed-matter physics, chemistry, and materials science. Typical problems in these fields often require computer simulations that involve a large number of atoms on extended time scales. Subjects of interest can, for example, be dislocations, grain boundaries and interfaces, disordered phases, liquids, or amorphous materials. Moreover, modeling of materials processes can include condensation processes, grain growth, bulk and surface diffusion, thin-film growth, cluster deposition, sintering, and crack growth, to name only a few. In order to treat such problems in a computationally efficient manner, while maintaining atomic resolution, analytical potential models that deliver realistic energies and interatomic forces are an indispensable tool for bridging the gap between quantum-mechanical methods and mesoscopic continuum models. However, modeling covalently bonded materials by means of analytical potentials is a very challenging task. In the past, numerous potential models[7–12] for semiconductors have been proposed including cluster potentials or cluster functionals of Keating- or bond-order type. However, none of them has emerged as being clearly superior to the others.

By far the most widely employed potential for silicon carbide is the bond-order potential (BOP) by Tersoff[13] (T89). The pair parameters are obtained by averaging the parameters for the elements, while the three-body parameters depend only on the type of the pivot atom. Tersoff's parameter sets have been supplemented by Beardmore and Smith[14] to enable atomistic modeling in the Si—C—H system. Dyson and Smith[15,16] (DS) employed the Brenner potential scheme to derive parameter sets fitted to reproduce the properties of small molecules and surfaces. Modified versions of Tersoff's potential that were optimized for specific applications have been published, e.g., by Gao and Weber[17] and by Devanathan *et al.*[18] Although these potentials are well suited for certain applications, like modeling of surfaces, molecules,[14,15] or structural transformations,[19] they are of limited use if the respective application requires a more extended sampling of configuration space. This holds equally true for a Keating-type potential proposed by Chatterjee *et al.*[20] and Shimojo *et al.*[19] that was complemented by electrostatic contributions for studying the sintering of nanocrystalline silicon carbide and structural transformations under pressure.

In this study, we are mainly interested in developing a potential for atomic scale simulations of processes which involve transitions between widely different atomic configurations, such as those encountered, for instance, during the inert gas condensation of silicon-carbon nanoparticles.[21] In in the course of this work we have derived parameters for the Si—C interaction, but also revisited established parametrizations for silicon and carbon and finally refined the parameter sets for the Si—Si and C—C interaction, too. Using a systematic fitting approach our model follows the same scheme that was previously applied to GaAs and GaN.[22,23]

II. METHODOLOGY

Bond-order potentials[24] are approximations of the moment expansion within the tight-binding scheme[25] and therefore close relatives to the embedded-atom method.[22,26] The functional form used in the present work has been successfully applied for modeling of semiconductors[18,22,23] and proven to be suitable for the description of metals and metal carbides, too.[12] Therefore only the basic formulas are given here. The cohesive energy is written as a sum over individual bond energies,

TABLE I. Parameter sets for silicon, carbon, and silicon carbide as derived in this work. The parameter set Si-I is recommended for simulations with SiC while Si-II yields an improved description of elastic and thermal properties of elemental silicon.

	Si-I	C	Si—C	Si-II
D_0 (eV)	3.24	6.00	4.36	3.24
r_0 (Å)	2.232	1.4276	1.79	2.222
S	1.842	2.167	1.847	1.57
β (Å^{-1})	1.4761	2.0099	1.6991	1.4760
γ	0.114354	0.11233	0.011877	0.09253
c	2.00494	181.910	273987	1.13681
d	0.81472	6.28433	180.314	0.63397
h	0.259	0.5556	0.68	0.335
2μ (Å^{-1})	0.0	0.0	0.0	0.0
R (Å)	2.82	2.00	2.40	2.90
D (Å)	0.14	0.15	0.20	0.15

$$E = \sum_{i>j} f_C(r_{ij}) \left[V_R(r_{ij}) - \underbrace{\frac{b_{ij} + b_{ji}}{2}}_{\bar{b}_{ij}} V_A(r_{ij}) \right] \quad (1)$$

with the pairwise attractive and repulsive contributions given by

$$V_R(r) = \frac{D_0}{S-1} \exp[-\beta\sqrt{2S}(r - r_0)] \quad (2)$$

and

$$V_A(r) = \frac{SD_0}{S-1} \exp[-\beta\sqrt{2/S}(r - r_0)], \quad (3)$$

where D_0 and r_0 are the dimer energy and bond length. The parameter β can be determined from the ground-state oscillation frequency of the dimer,[12] while S is adjusted to the slope of the Pauling plot. The cutoff function

$$f_C(r) = \begin{cases} 1 & r < R - D \\ \frac{1}{2} - \frac{1}{2}\sin\left(\frac{\pi}{2}\frac{r-R}{D}\right) & |R - r| \leq D \\ 0 & R + D < r \end{cases} \quad (4)$$

restricts the interactions to the first neighbor shell. The parameters R and D specify the position and the width of the cutoff region. The bond-order is given by

$$b_{ij} = (1 + \chi_{ij})^{-1/2} \quad (5)$$

with

$$\chi_{ij} = \sum_{k(\neq i,j)} f_C(r_{ik}) \exp[2\mu(r_{ij} - r_{ik})] g(\theta_{ijk}) \quad (6)$$

and the angular function

$$g(\theta) = \gamma\left(1 + \frac{c^2}{d^2} - \frac{c^2}{d^2 + [h + \cos\theta]^2}\right). \quad (7)$$

The three-body interactions are determined by the parameters 2μ, γ, c, d, and h, which leads in total to up to nine adjustable parameters, all of them depending on the type of atoms i and j. The parameter set for every interaction type is fitted independently using our fitting code PONTIFIX.[27]

The parameter optimization proceeds as follows: First, the pair parameters are adjusted to the dimer properties (D_0, r_0, β) and the slope of the Pauling plot (S). Thereafter, the three-body parameters are fitted to the cohesive energies and bond lengths of several high-symmetry structures as well as to the elastic constants of the ground structures. The transferability of the potential is enforced by including a variety of differently coordinated structures in the fitting database. Further details regarding the fitting procedure can be found in Refs. 12 and 22.

The parameter sets used in this study are compiled in Table I. For simulations in the context of silicon carbide, it is recommended to use the parameter set Si-I which has been extensively tested for this purpose. The alternative parameter set Si-II provides an improved description of the elastic and thermal properties of elemental silicon.

III. SILICON

For silicon there are various well tested potentials available in literature (e.g., Refs. 7, 9, and 28) and therefore yet another potential seems to be redundant. Bond-order potentials for silicon, however, that are compatible with our formalism have only been proposed by Tersoff[28] as well as Dyson and Smith.[15] While the parameter set given by Tersoff[28] suffers from an underestimation of the dimer binding energy and therefore is not satisfactory for the description of small molecules, the silicon parameter set derived by Dyson and Smith[15] is not optimized for bulk properties. Therefore we decided to newly adjust parameters for the Si—Si interaction.

TABLE II. Silicon dimer properties: Experiment data in comparison with the new bond-order potential and the potentials by Dyson-Smith (DS), Tersoff (T3), and Stillinger-Weber (SW). D_0 is the binding energy, r_0 the equilibrium bonding distance, and k the wave number of the ground state. S is the slope parameter.

	Expt.	This work		Other potentials		
				DS	T3	SW
	Ref. 29	Si-I	Si-II	Ref. 15	Ref. 28	Ref. 30
r_0 (Å)	2.246	2.232	2.222	2.197	2.295	2.352
D_0 (eV)	3.24	3.24	3.24	3.39	2.67	2.32
k (cm^{-1})	511	522	556	532	471	462
S	1.91[a]	1.84	1.57	1.41	1.43	

[a]Fitted to bond length and energy of the dimer and silicon in the diamond structure, cf. Ref. 24.

A. Dimer properties

For the silicon dimer the binding energy D_0, the equilibrium bonding distance r_0 and the wave number k of the ground-state oscillation, which can be directly related to the potential parameter β, are experimentally known[29] and could be directly taken as potential parameters. However, since β and r_0 also affect the energy-volume curves of the bulk structures, minor adjustments of β and r_0 were necessary in order to improve the agreement with experimental data.

A compilation of dimer properties for the parameter sets presented in this work (Si-I, Si-II) with experimental data and the potentials by Dyson-Smith (DS), Tersoff (T3), and Stillinger-Weber (SW) is given in Table II. The correct dimer

binding enters directly into the new parameter sets for Si, while r_0 and β are chosen to closely reproduce the experimental data.

B. Bulk properties

Silicon like several other covalently bonded materials (GaAs, SiC) exhibits a negative Cauchy discrepancy ($c_{12}-c_{44}<0$). When the diamond lattice is sheared, internal relaxation occurs by displacement of the two fcc sublattices with respect to each other along the $\langle 111 \rangle$ direction. The Kleinman parameter ζ measures the displacement in units of the nearest-neighbor distance.[31–33] The shear modulus c_{44}^0 of the unrelaxed structure can only be obtained from first-principles calculations. The difference between the relaxed (c_{44}) and unrelaxed (c_{44}^0) shear moduli is related to the transverse optical phonon frequency at the Γ point.[33]

Bazant et al.[34] introduced figures of merit for the description of the elastic constants by analytical potentials. They are defined as

$$\alpha_H = (7c_{11}+2c_{12})c_{44}/3(c_{11}+2c_{12})(c_{11}-c_{12}) \quad (8)$$

and

$$\alpha_B = (4c_{11}+5c_{12})/9c_{44}^0. \quad (9)$$

For the experimental data, α_H and α_B are close to 1. The corresponding values are included in Table III, which summarizes the properties of silicon in its equilibrium structure.

The parameter set Si-I provides an excellent description of the properties of the diamond lattice with the single exception of a somewhat larger deviation in c_{44} leading to a

TABLE III. Properties of silicon in its equilibrium structure from experiment, quantum-mechanical (QM) methods such as density-functional theory (DFT), as well as tight binding (TB) calculations and for various analytical potentials [DS: Dyson and Smith (Ref. 15), LSA: Lenosky et al. (Ref. 35), EDIP: Bazant et al. (Ref. 9), SW: Stillinger and Weber (Ref. 7), T3: Tersoff (Ref. 28)]. a_0: lattice constant; E_c: cohesive energy; B and B': bulk modulus and its pressure derivative, respectively; c_{ij}: elastic constants; c_{44}^0: static (unrelaxed) shear modulus; α_H and α_B: figures of merit (see text for definition and discussion), ζ: Kleinman parameter.

	Expt.	QM methods		This work		Other analytical potentials				
		DFT	TB	Si-I	Si-II	DS	LSA	EDIP	SW	T3
	Ref. 36	Ref. 37	Ref. 38			Ref. 15	Ref. 35	Ref. 9	Ref. 30	Refs. 28 and 30
a_0 (Å)	5.429	5.400	5.429	5.429	5.429	5.432	5.430	5.430	5.431	5.432
E_c (eV/atom)	−4.63		−4.62	−4.63	−4.63	−4.63	−4.61	−4.65	−4.63	−4.63
B (GPa)	99	93	100	99	99	98	110	99	108	98
B'	4.20	3.8		4.43	4.36				2.93	4.30
c_{11} (GPa)	168	159	167	167	167	109	165	175	162	143
c_{12} (GPa)	65	61	67	65	65	93	82	62	82	75
c_{44} (GPa)	80	85	75	60[a]	72[a]	38[b]	72	71	60	69
c_{44}^0 (GPa)		111		105	111	114[b]		112	117	119
$c_{12}-c_{44}$ (GPa)	−15	−24	−8	5	−7	55	10	−9	22	6
α_H	1.14	1.27	1.08	1.02	1.03	2.55	1.15	0.94	1.00	1.34
α_B	0.98	0.94		1.06	0.99	0.88	1.00	1.00	0.89
ζ	0.54	0.53		0.54[a]	0.52[a]	0.91			0.63	0.67

[a]c_{44} and ζ calculated at an elastic strain of $\gamma=0.001$.
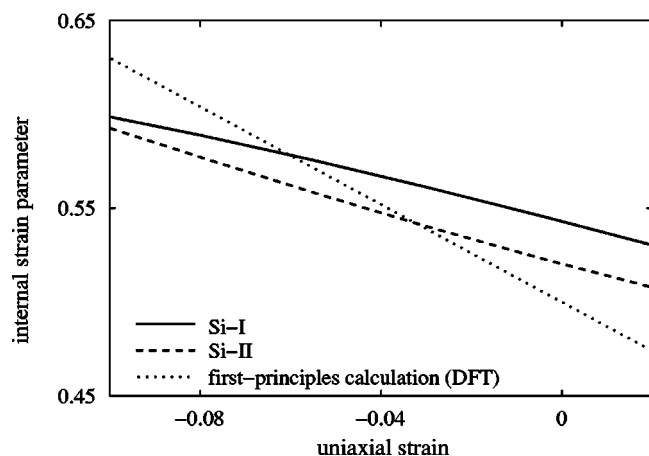[b]Calculated in the present work.

FIG. 1. Strain dependence of the Kleinman parameter in comparison to DFT results (Ref. 36).

positive Cauchy difference, $c_{12} - c_{44}$. The negative Cauchy discrepancy is correctly reproduced by the Si-II parametrization while maintaining the excellent agreement with the other elastic properties.

We have also evaluated the strain dependence of the Kleinman parameter as shown in Fig. 1. With both parameter sets for silicon an increase of the internal strain parameter is found with increasing uniaxial strain, which is in line with theoretical results obtained by density-functional theory calculations,[37] although slight deviations of the slope have to be acknowledged.

C. Coordination

Silicon exhibits a plethora of high-pressure phases with very small energy differences, and the corresponding region of the phase diagram is still not fully understood.[39–41] Many different crystalline phases in the pressure range up to 248 Gpa have been predicted, which are partly metasable at atmospheric pressures. If transition paths are considered, the situation becomes even more intricate. In fact, some phases are only accessible after a certain squence of temperature and pressure treatments. With increasing pressure the respective equilibrium phases exhibit larger coordinations and behave increasingly metallic. The description of these structurs imposes a stringent test on the transferability of the potential model presented in this work.

Table IV presents a compilation of structural data from density-functional theory (DFT) calculations in comparison with several analytical potentials. The energetic ordering of

TABLE IV. Properties of several experimentally observed and hypothetical structures of silicon. DIA: diamond, SH: simple hexagonal, SC: simple cubic, BCC: body-centered cubic, FCC: face-centered cubic. E_c: cohesive energy; ΔE: energy difference with respect to diamond structure; a: lattice constant; c/a: axial ratio for noncubic structures; x: internal parameter of the $bc8$ structure. Energies are given in eV/atom, lattice constants in Å. Structures marked with an asterisk (*) were included in the fitting database.

		QM methods	This work		Other analytical potentials				
		DFT Refs. 9, 30, 42, and 43	Si-I	Si-II	DS Ref. 15	LSA Ref. 35	EDIP Ref. 9	SW Ref. 30	T3 Ref. 30
DIA* (A4)	E_c	−4.670/−4.650	−4.630	−4.630	−4.634	−4.612	−4.650	−4.630	−4.630
	a	5.451/5.43	5.429	5.429	5.431	5.429	5.430	5.431	5.432
BC8	ΔE	0.130/0.085	0.230	0.250		0.080		0.201	0.245
	a	6.67/6.577	6.625	6.655				6.591	6.644
	x	0.100	0.101	0.099	0.103			0.102	0.101
β-TIN (A5)	ΔE	0.266/0.210	0.412	0.444	0.760	0.310	0.67	0.213	0.327
	a	4.822/4.730	4.856	4.896	4.810	4.597	4.760	4.969	4.905
	c/a	0.552	0.527	0.525	0.543	0.555	0.550	0.561	0.524
SH (A$_f$)	ΔE	0.293	0.476	0.515	0.64	0.230		0.403	0.469
	a	2.639	2.659	2.670	2.69	2.544		2.833	2.699
	c/a	0.940	0.965	0.986	0.99	0.925		0.918	0.967
SC* (A$_h$)	ΔE	0.348	0.397	0.537	0.339	0.290	0.532	0.293	0.318
	a	2.528	2.525	2.553	2.546	2.404	2.503	2.612	2.544
BCC* (A2)	ΔE	0.525	0.503	0.431	0.629	0.720	1.594	0.300	0.432
	a	3.088	3.043	3.063	3.107	3.135	3.243	3.245	3.084
FCC* (A1)	ΔE	0.566	0.587^a	0.575	1.08	0.700	1.840	0.423	0.761
	a	3.885	3.940	3.989	3.91	4.008	4.081	4.147	3.897

^{a}These values for the cohesive energy and the lattice constant have been obtained with $R = 2.90$ Å and $D = 0.15$ Å. If the values from Table I are used the bond length intersects the cutoff region whence the cohesive energy is reduced and the structure becomes unstable.
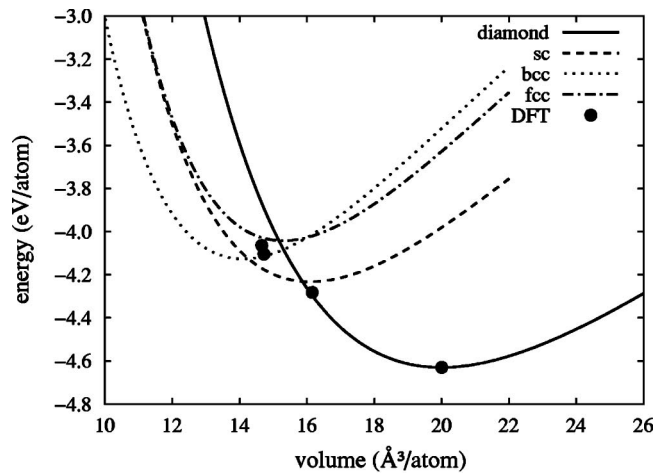
(a)
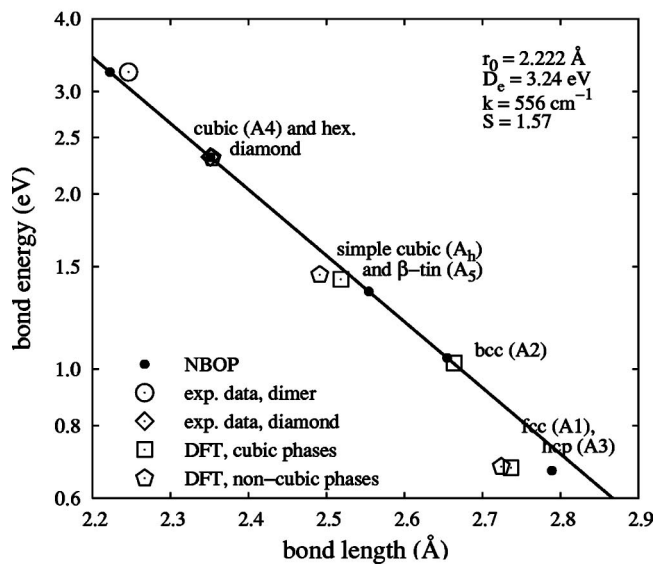
(b)

FIG. 2. Pauling plot (top) and energy-volume curves (bottom) for the parameter set Si-I in comparison with experimental (Refs. 29 and 35) and data from density-functional theory (DFT) calculations (Ref. 42).

the structures is very difficult to reproduce due to the extremely small energy differences between the competing structures. Our first parametrization (Si-I) for the silicon potential, however, provides a good overall description of the structural properties of the higher-coordinated structures as illustrated by the Pauling plot and the energy-volume curves shown in Fig. 2. With respect to the high-pressure phases it is therefore comparable to or even better than alternative potentials from literature.

D. Thermal properties

The experimental melting point of silicon is 1687 K.[44] The liquid phase is denser than the crystalline phase at the melting point and the solid-liquid phase transition is accompanied by an increase in average coordination. There are several methods to determine the melting point from molecular-dynamics simulations (cf. Refs. 45 and 46, and references therein). In this work we have set up a system comprising a liquid and a crystalline phase separated by a sharp (100) interface. The system was equilibrated at various temperatures using a Berendsen-type thermostat, while the pressure was kept at 0 kbar by employing a Berendsen-type barostat.[47] Steady-state conditions were assumed when the potential energy fluctuated about a constant value. The melting point is the temperature at which the interface is stable with the liquid and crystalline phases in equilibrium. This method avoids hysteresis effects which occur when the melting and solidification of a single phase system is simulated.

The melting temperature has been determined as 2450 ± 50 K for the Si-I parameter set and 2150 ± 25 K for the Si-II parameter set. These values are considerably higher than the experimental melting point of 1687 K, but better than 2550 ± 50 K obtained by us and 2547 ± 22 K reported by Cook and Clancy[46] for Tersoff's bond-order potential. The overestimation of the melting point, however, appears to be a general problem inherent to bond-order potentials for semiconductors (see, e.g., Ref. 22), while in case of elemental metals, like Pt (Ref. 12) and Zn,[48] perfect agreement with experimental results was achieved using the same bond-order formalism.

TABLE V. Thermal properties of several analytical silicon potentials in comparison with experiment. T_m: melting point; ΔH_m: transition enthalpy of melting; ΔH_{l-c}: enthalpy difference between the material in the crystalline state at 0 K and the molten material at the melting point; ρ_l, ρ_s: density of the liquid and solid phase at the melting point; $\Delta \tilde{\rho}$: relative change of density upon melting defined as $\Delta \tilde{\rho} = (\rho_l - \rho_s)/\rho_s$.

	Expt.[a]	Si-I	Si-II	T3	SW
T_m (K)	1687	2450 ± 50	2150 ± 25	2547 ± 22[b]	1688 ± 26[b]
ΔH_m (kJ/mole)	50.2	49.5 ± 0.2	48.4 ± 0.2	40.8 ± 0.2	31.3
ΔH_{l-c} (kJ/mole)	~ 93.4[c]	82.4	78.9	73.7	88.7
ρ_l (g/cm³)	2.51	2.30	2.40	2.28	2.47
ρ_s (g/cm³)	2.30	2.25	2.26	2.25	2.29
$\Delta \tilde{\rho}$ (%)	9.1	2.2	6.2	1.3	8.1

[a]Reference 35.
[b]Reference 46.
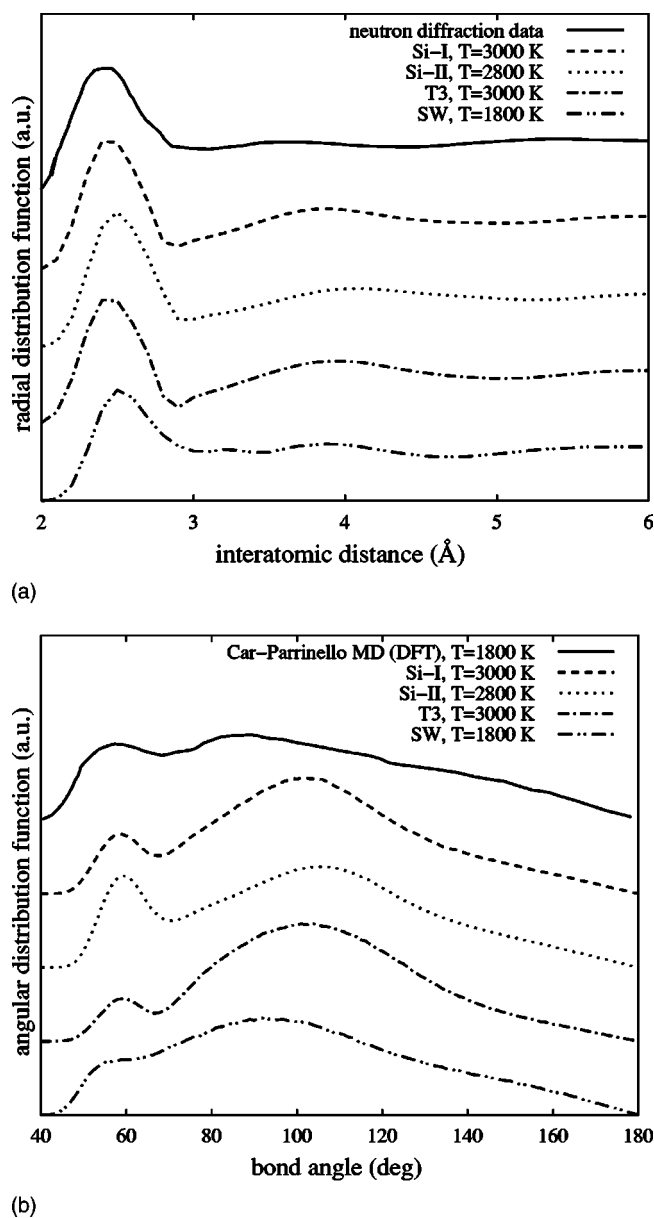[c]Reference 49.

(a)

(b)

FIG. 3. Radial (left) and angular (right) distribution functions from experiment (Ref. 36) and first-principles calculations (Ref. 49) in comparison with analytical potentials.

The melting and other thermal properties are summarized in Table V together with experimental data. Most prominently, the transition enthalpy and the relative change of the density are in very good agreement with experimental data for the parametrization Si-II. Here it should be noted that none of these properties have been part of the reference database which gives evidence for the transferability of the potential.

Next, the structure of the molten phase was characterized by calculating the radial and angular distribution functions as shown in Fig. 3. The radial distribution functions for all analytical potentials considered here are in good agreement with experiment. The most notable difference is the dip between the first and second coordination shell observed for the new parameter sets as well as for the Tersoff potential. This fea-

ture is a result of the steep cutoff function between the first and second nearest-neighbor shell [Eq. (6)] which leads to strong forces on atoms within the cutoff region. However, it can hardly be avoided without compromising other potential properties.

In contrast to the radial distribution functions, a more diverse behavior is displayed by the angular distributions. First-principles calculations[49] predict two distinct maxima at $\sim 60°$ and $\sim 90°$. In agreement with previous studies[50] the bond-order potentials for silicon reproduce this feature while the SW potential exhibits only a shoulder at about 60° but no maximum. Although the melting point is overestimated, the Tersoff-type as well as our silicon potentials realistically describe the structure of the molten phase.

Finally, we estimated the linear thermal-expansion coefficient close to the melting point to be $\alpha_L = 5 \pm 2$ μK^{-1} which compares well with the value of $\alpha_L = 4.66$ μK^{-1} obtained by extrapolation of experimental data to the melting point.[36] Again, the good agreement with experimental and first-principles data (with the exception of the melting point) gives further hindsight for the transferability of the bond-order potential scheme, since none of these properties were considered during the fitting process.

E. Point defects

Point defects in silicon have been extensively studied, both experimentally and theoretically, over the last decades.[51,52] Since energetic and structural properties of point defects are experimentally difficult to assess, quantum-mechanical total-energy calculations have been an invaluable tool in resolving the situation. Strain fields around point defects, various charge states, and intricate electronic interactions render such calculations a nontrivial task (see, e.g., Refs. 51 and 53). By now, there is consensus that the dumbbell $\langle 110 \rangle$ interstitial has the lowest formation energy followed by the hexagonal and tetrahedral configurations (Ref. 51 and references therein). For these investigations quantum-mechanical calculations have been performed at zero temperature and pressure. The situation at nonzero temperatures is even more difficult to resolve, because the ordering can change completely due to different vibrational properties of the various point defect configurations and the related contributions to entropy.

It has turned out to be very difficult to capture the results of quantum-mechanical calculations in analytical potential models. Recently, a potential model has been proposed that is optimized for point defects and amorphous structures (EDIP),[9] but exhibits deficiencies as it comes to the description of higher coordinated structures (Table IV). An overview of the formation energies of the point defects in silicon is given in Table VI. Among the established analytical potentials only the EDIP and the SW potentials reproduce the dumbbell, while the silicon potentials presented in this work favor the tetrahedral position. By varying the cutoff distances within the parameter set Si-I, however, the picture is slightly changed and the hexagonal position becomes the lowest energy configuration.

The structural stability of the dumbbell configuration was tested in molecular dynamics runs over 0.5 ns at various

TABLE VI. Formation energies[a] in units of eV for relaxed point defects from *ab initio* and tight-binding calculations in composition with analytical potentials. V: vacancy; I_H: hexagonal interstitial; I_T: tetragonal interstitial; I_D: $\langle 110 \rangle$ dumbbell interstitial.

| | QM methods | | | This work | | | Other analytical potentials | | | |
| | DFT | | TB | | | | EDIP | SW | T3 | LSA |
	Ref. 51	Ref. 54	Ref. 38	Si-I	Si-I[b]	Si-II	Ref. 9	Ref. 30,34,82	Ref. 30,82	Ref. 35
V	2.8–4.1	3.17	3.68	3.2	3.2	3.2	3.22	2.82	3.70	3.30
I_T	4.0		3.75	3.5	4.4	3.2	4.05	5.25	3.45	3.00[c]
I_H	3.8	3.31	4.03	4.0	4.1	3.3	4.16	6.95	4.61	3.21
I_D	3.7	3.31	3.46	4.4	4.7	3.9	3.35	4.68,~3.9[d]	4.4	3.13

[a]The defect formation enthalpies for the new potential have been calculated by allowing full, i.e., internal and volume relaxations, while in the DFT calculations typically only internal relaxations are taken into account.
[b]With modified cutoff, $R=2.90$ Å and $D=0.15$ Å.
[c]Relaxed configuration with interstitial atom displaced from the tetragonal towards the hexagonal interstitial site. The formation enthalpy is 3.11 eV if the symmetry is fixed.
[d]Extended split-interstitial configuration.

temperatures. We observed the dumbbell interstitial configuration to be metastable up to ~400 K. At temperatures above this threshold it dissembled into the hexagonal interstitial configuration.

Keeping in mind that the present potential has not been optimized for point defects, reasonable agreement with the results of quantum-mechanical calculations is obtained, although the dumbbell interstitial is not the most stable interstitial defect. The cutoff parameters are found to have an immediate effect on the formation energies. A systematic investigation of this interplay is recommended if the optimization of this potential for simulations of points defects is intended.

F. Conclusive remarks on the Si parametrization

The newly parametrized bond-order potentials for silicon (Si-I and Si-II) provide excellent models for the elastic properties of the diamond phase and reproduce structure and energetics of the dimer as well as high pressure phases very well. For the liquid-solid transition, both enthalpy and density changes are properly reproduced and even the angular distribution function of the molten phase is in agreement with predictions from first-principle calculations. There is obvious disagreement, however, if formation enthalpies of point defects are compared with results based on first-principles calculations. Other properties, like one- and two-dimensional defects, were not tested in this work, but might be an interesting subject for further studies.

IV. CARBON

The carbon (C—C) parameter sets proposed by Brenner[11] allow for a good description of the properties of hydrocarbon molecules, however, they yield only a mediocre model for the bulk phases of carbon. In particular, the elastic constants of diamond are poorly reproduced. Thus we decided to derive C—C parameters that properly predicts the elastic properties, while maintaining most of the features of the original parametrization. The new parameter set almost retains the

dimer parameters of the Brenner potential while at the same time delivers a description of the bulk phases which is comparable to the Tersoff potential.[55]

A. Dimer properties

The dimer properties are summarized in Table VII. The dimer energy D_0 and wave number k for the new carbon potential are very similar to the second parametrization of the original Brenner potential.[11] The bond length is somewhat longer, which turned out to be necessary in order to obtain a better model for the bulk phases. The Tersoff potential underestimates the dimer energy by about 14%, similar to the case of silicon. All potentials yield a somewhat too low wave number k, as compared to the experimental value. For the potentials considered this deficiency cannot be overcome without accepting a considerable deviation in the elastic moduli of the bulk phases.

B. Bulk properties

Carbon naturally occurs in the graphite as well as diamond structures, in which the atoms are sp^2 and sp^3 hybridized, respectively. At ambient conditions graphite is slightly more stable than diamond with the difference in the cohesive energies of the two structures being on the order of meV.

TABLE VII. Carbon dimer properties: Experimental data in comparison with the new bond-order potential (this work) and the potentials by Brenner (parameter set II in Ref. 11) and Tersoff. D_0 is the binding energy, r_0 the equilibrium bonding distance, and k the wave number of the ground state. S is the slope parameter.

	Expt. Ref. 29	This work	Brenner-II Ref. 11	Tersoff Ref. 55
D_0 (eV)	6.21	6.00	6.00	5.17
r_0 (Å)	1.243	1.428	1.390	1.447
k (cm^{-1})	1855	1482	1548	1343

TABLE VIII. Properties of diamond and graphite calculated with the new carbon parametrization in comparison with experiment, density-functional theory calculations (DFT) and the potentials by Brenner (parameter set II in Ref. 11) and Tersoff. ΔE: energy difference with respect to graphite modification; a: lattice constant (in plane lattice constant in the case of graphite); A: Zener anisotropy ratio; $A = 2c_{44}/(c_{11} - c_{12})$. For the interpretation of the remaining symbols see Table III.

	Expt. Ref. 44	DFT Refs. 56 and 57	This work	Brenner-II Ref. 11	Tersoff Ref. 55
Graphite (A9)					
a (Å)	2.46	2.440–2.47	2.555	2.513	2.530
E_c (eV/atom)	−7.374	−9.027−−9.001	−7.374	−7.376	−7.396
B (GPa)	286–319	236–319	232[a]	258[a]	225[a]
B'		3.57, 3.58	4.00	3.97	3.83
Cubic diamond (A4)					
a (Å)	3.567	2.528–3.55	3.566	3.558	3.566
ΔE (eV/atom)		−0.0028−+0.0004	0.0009	0.0524	0.0250
B (GPa)	444	444–494	445	484	425
B'	~4	2.60–3.67	4.15	4.06	3.92
c_{11} (GPa)	1081	1100	1082	621	1067
c_{12} (GPa)	125	143	127	415	104
c_{44} (GPa)	579	587	635	383	636
c_{44}^0 (GPa)			673	642	671
ζ		0.107	0.21	0.76	0.22
α_H	1.19	1.18	1.30	2.21	1.33
α_B			0.82	0.79	0.79
A	1.21	1.23	1.33	3.72	1.32

[a]Evaluated using the experimental c/a ratio to determine the atomic volume.

Graphite consists of sp^2 bonded sheets which are held together by van der Waals forces. Within the short-ranged bond-order potential model these long-ranged interactions are not properly accounted for, a deficit which can be fixed by adding a weak long-range pair potential. These interactions are crucial for reproducing the layer separation and the elastic response of the material perpendicular to the layers, but they have a negligible effect on the energetics and the atomic separations within the graphite sheets. As shown in Table VIII the carbon potential exactly reproduces the experimental cohesive energy of the graphite structure. The lattice constant is also in good agreement with experimental observations. Since the energy difference between the graphite and diamond structures is not exactly known, we have decided to employ an approximate value of 1 meV in the fitting database, which is on the order of magnitude expected from experimental and theoretical experience. This energy difference as well as the lattice constants is properly described using the new carbon parametrization. Most importantly, elastic constants are in very good agreement with experiment fixing a problem of Brenner's original parametrization. In principle, the C—C parameters should also work together with the C—H parameters of Brenner's original hydrocarbon potential. Here, however, we only tested the overbinding corrections in the context of point defects as discussed in Sec. IV D.

C. Coordination

Furthmüller *et al.* have presented an extensive work on the energetics and structure of various solid modifications of carbon. Some of these structures entered our fitting database, while some served as tests for the transferability of the potential. The cohesive energies and structural parameters are compiled in Table IX.

The carbon potential provides a good overall description of the low as well as high coordinated structures. Naturally, particular attention has been paid to obtain exact agreement for the graphite and diamond phases. The good agreement with experiment and DFT calculations is further demonstrated in the Pauling plot shown in Fig. 4 which illustrates the variation of the bond energy with bond length.

D. Point defects

Experimentally, the formation enthalpy of the carbon vacancy in diamond has not been determined yet, but there are a few theoretical studies (see Ref. 58 and references therein). A theoretical treatment of this defect is not trivial since many-electron correlation, coupling between the defect and the surrounding bulk material as well as Jahn-Teller distortions have to be accounted for. Only recently a diffusion Monte Carlo (DMC) study has been performed by Hood and co-workers[58] who reported a vacancy formation energy of

TABLE IX. Properties of several experimentally observed and hypothetical structures of carbon. Results obtained with the new carbon potential are compared with experiment, density-functional theory calculations (DFT, Ref. 56), and the potentials by Brenner (second parameterization, Ref. 11) and Tersoff (Ref. 55); ΔE: energy difference with respect to graphite modification, GRA: graphite, see Table IV for the interpretation of the remaining symbols.

	Expt. Ref. 44	DFT Ref. 56	This work	Brenner-II Ref. 11	Tersoff Ref. 55
GRA* (A9)					
a (Å)	2.46	2.440–2.47	2.555	2.513	2.530
E_c (eV/atom)	−7.374	−9.027–−9.001	−7.374	−7.376	−7.396
DIA* (A4)					
a (Å)	3.567	2.528–3.55	3.566	3.558	3.566
ΔE (eV/atom)		−0.0028–+0.0004	0.0009	0.0524	0.0250
BC8					
a (Å)		4.419–4.51	4.429	4.351	4.437
x		0.0943–∼0.1003	0.0963	0.1019	0.0965
ΔE (eV/atom)		0.689–0.691	0.772	0.446	0.775
β-TIN (A5)					
a (Å)		3.310	3.425	3.660	3.555
c/a		0.390	0.435	0.380	0.436
ΔE (eV/atom)		2.727–2.82	3.452	1.379	3.779
SC* (A_h)					
a (Å)		1.744–1.770	1.783	1.744	1.802
ΔE (eV/atom)		2.60–2.66	3.297	2.133	2.974
BCC* (A2)					
a (Å)		2.326–2.375	2.160	2.093	2.152
ΔE (eV/atom)		4.24–4.351	3.964	3.037	3.771
FCC* (A1)					
a (Å)		3.021–3.078	2.859	1.863	2.728
ΔE (eV/atom)		4.50–4.648	4.483	3.713	4.411

5.96±0.34 eV. The vacancy formation enthalpy calculated with the new carbon potential is 3.09 eV, which is considerably lower than the *ab initio* value. However, this deficiency is clearly related to the missing overbinding corrections which are needed in order to balance the coordination change in the first neighbor shell of the vacancy. In fact, a similarly low value is found for the Tersoff potential as well. If the overbinding corrections as originally parametrized by Brenner are included, we obtain a vacancy formation enthalpy of 5.24 eV in very good agreement with theory.

The formation energies/enthalpies for interstitial defects in diamond are very large (see Table X). DFT calculations suggest values of ∼16 eV and larger from which it has been concluded that these defects are not relevant for the process of diffusion in diamond.[59] The new bond-order potential yields reasonable values for the formation enthalpies of these defects regardless whether overbinding corrections are included or not.

V. SILICON CARBIDE

Silicon carbide occurs in more than 200 different polytypes, which differ in the stacking sequence of the Si—C bilayers[60] and are classified as either cubic (*C*), hexagonal (*H*), or rhombohedral (*R*). The most abundant polytypes are 3*C* (zinc blende), 6*H*, 4*H*, and 2*H* (wurtzite). The energy differences between the different polytypes are extremely small. Park *et al.*[61] determined the energetic ordering of the four most abundant types as 4*H*, 6*H*, 3*C*, and 2*H* and calculated a maximum energy difference of only 4.3 meV/atom. Since our model is restricted to first neighbor interactions, the various polytypes energetically cannot be distinguished. However, this does not seem a severe restriction, because entropic contributions to the free enthalpy will dominate at nonzero temperatures.

A. Dimer properties

The dimer properties are experimentally not well known. Huber and Herzberg[29] report an upper limit for the dimer
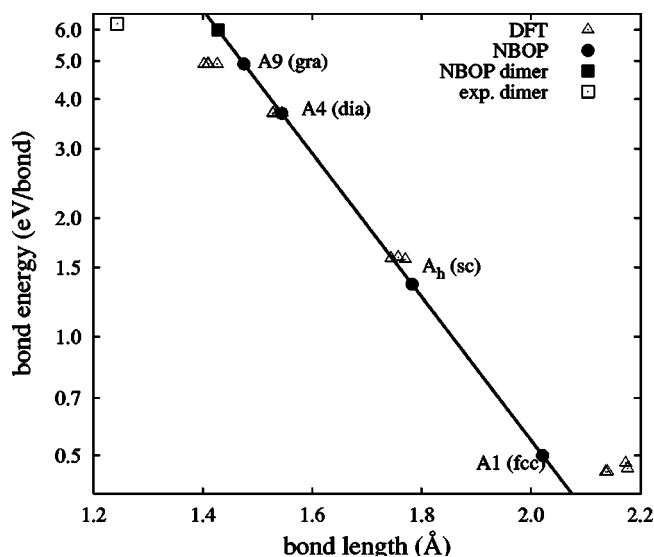
FIG. 4. Pauling plot for the new carbon parameter set. The straight line indicates the Pauling relation.

binding energy of 4.64 eV and and a bond length of approximately 1.82 Å. Ground-state frequencies of the dimer are given in a number of *ab initio* studies.[62–64] The reported values, however, vary appreciably, which in connection with the experimental data induces some degree of freedom in adjusting the dimer parameters.

Table XI summarizes the data from literature, our SiC parametrization, and the dimer properties of Tersoff's SiC potential (T89). The latter yields a ground-state frequency which is more than 25% lower than the values of quantum-mechanical calculations, while the new SiC potential delivers a values that is very close to the reference data.

B. Bulk properties

Despite the large technological interest in the mechanical properties of silicon carbide, the elastic constants of cubic

TABLE X. Formation energies (DMC, DFT)/enthalpies (analytical potentials) of point defects in carbon in units of eV taken from diffusion Monte Carlo (DMC, Ref. 58) and density-functional theory (DFT, Refs. 58 and 59) calculations in comparison with the new potential and the established potentials by Brenner (second parameterization, Ref. 11) and Tersoff (Ref. 55). Values in brackets denote formation enthalpies obtained without overbinding corrections. V_C: single vacancy; I_T: tetrahedral interstitial; I_S: $\langle 100 \rangle$ split interstitial; I_B: bond-centered interstitial (see Ref. 59 for interstitial defect geometries).

	DMC Ref. 58	DFT Ref. 59	This work	Brenner-II Ref. 11[a]	Tersoff Ref. 55[a]
V_C	5.96±0.34	6.98, 7.2	5.24 (2.59)	8.84 (1.84)	3.42
I_T		23.6	23.90 (23.69)	9.08 (9.05)	19.42
I_S		16.7	10.21 (9.58)	5.36 (3.98)	9.93
I_B		15.8	16.06 (14.90)	9.15 (9.47)	14.46

[a]The formation enthalpies given here have been calculated in the context of the present work.

TABLE XI. Comparison of dimer properties of SiC. D_0: bond energy; r_0: bond length; k ground-state oscillation frequency.

	Expt. Ref. 29	*Ab initio* Ref. 62	*Ab initio* Ref. 63	This work	T89 Ref. 13
D_0 (eV)	≤4.64	4.36		4.36	4.20
r_0 (Å)	~1.82	1.726	1.726	1.79	1.77
k (cm^{-1})		959	927	902	691

silicon carbide have not been consistently determined yet.[65] Apparently, the best data at hand are the elastic constants given by Lambrecht *et al.*,[66] which have been obtained by transformation of experimental data for hexagonal polytypes. These values have been employed in fitting the potential. In a recent theoretical study,[67] which appears to be the most accurate to date, elastic constants in excellent agreement with the values determined by Lambrecht *et al.* have been reported.

A compilation of published data is given in Table XII including results obtained with our SiC potential and with three different versions of the Tersoff potential (T89, T90, T94) for SiC and the potentials by Dyson and Smith (DS),[15] and by Gao and Weber (GW).[17] Obviously, the SiC parametrization of our bond-order potential reproduces all elastic constants very well, especially in comparison to alternative SiC potentials.

C. Coordination

The high-pressure phase diagram of silicon carbide is neither as complex nor as extensively explored as for silicon. It is well established that the zinc-blende (B3) modification transforms to the rocksalt (B1) structure under compression,[19,74] and there is evidence for a similar transition in the case of 6*H*-SiC.[75] The transition pressures and paths are, however, still a matter of discussion (cf. Ref. 76 with comments and replies).

Only few theoretical investigations of higher-coordinated structures have been published. Chang and Cohen[77] and Karch *et al.*[60] conducted density-functional theory (DFT) calculations on the zinc-blende (B3), rocksalt (B1), and cesium chloride (B2) structures, which were taken as reference data for the potential fitting in the present work. It has been found impossible, however, to find a reasonable fit for all solid structures while leaving the description of the elastic properties unaffected. As a compromise, a significant deviation of the cohesive energy of the rocksalt (B1) structure from the theoretical value was accepted. Figure 5 shows the Pauling plot including first-principles and experimental data, while Table XIII summarizes the structural properties calculated with the new SiC potential.

D. Point defects

The number of point defect configurations for silicon carbide which have been explored in the literature is quite large. There are two types of vacancies, namely the C and the Si

TABLE XII. Comparison of bulk properties of 3C-SiC obtained from experiment, theory, and analytical potentials. The symbols have the same meaning as in Table III. A: anisotropy; $A = 2c_{44}/(c_{11} - c_{12})$.

	Expt.		QM methods				This work	Other analytical potentials				
				DFT		TB						
			NFP[b]	LAPW[b]	PWPP[b]			T89[a]	T90[a]	T94[a]	DS	GW
	Ref. 66	Ref. 65	Ref. 67	Ref. 68	Ref. 69	Ref. 70		Ref. 71	Ref. 71	Ref. 71	Ref. 15[c]	Ref. 17[c]
a_0 (Å)	4.3596		4.3367	4.360	4.344	4.36	4.359	4.321	4.307	4.280	4.349	4.360
E_c (eV/atom)	−6.340				−7.415		−6.340	−6.165	−6.210	−6.434	−6.340	−6.412
B (GPa)	225	211	218	210/216[d]	222/219[d]	229	224	224	231	241	224	235
B'				3.71	3.88		4.16					
c_{11} (GPa)	390	352	385	384	390	372	382	437	426	447	243	254
c_{12} (GPa)	142	140	135	132	134	157	145	118	134	134	215	225
c_{44} (GPa)	256	233	257	241	253		240[e]	311	280	293	62	66
c_{44}^0 (GPa)			284		273	256	305					
ζ			0.41		0.38[f]		0.49[e]					
α_H	1.54	1.59	1.55	1.45	1.50		1.46	1.59	1.50	1.48	2.34	2.40
α_B			0.87		0.91	0.99	0.83					
A	2.06	2.20	2.06	1.91	1.98		1.98	1.68	1.92	1.87	4.43	4.55

[a]T89, T90, T94 refer to the three parameterizations of the C—C interactions given by Tersoff (Refs. 13, 72, and 73), following the nomenclature of Ref. 71.
[b]NFP: new full potential; LAPW: linear augmented plane waves; PWPP: plane-wave pseudopotential.
[c]Calculated in the present work.
[d]The first values have been obtained from a fit to the Murnaghan (Ref. 68) and the Vinet (Ref. 69) equation of state, respectively, while the second values have been calculated using the relation $B = (c_{11} + 2c_{12})/3$.
[e]c_{44} and ζ calculated at an elastic strain of $\gamma = 0.001$.
[f]Geometric average of three independently calculated values.

vacancies (V_{Si}, V_C), and also two types of antisite defects (Si_C, C_{Si}). Furthermore, various different self-interstitial defect structures have been considered.[78,79] A tetrahedrally coordinated carbon interstitial can be surrounded either by four carbon (C_{TC}) or four silicon atoms (Si_{TS}) and equivalently for silicon. Four possible configurations can be studied for

FIG. 5. Pauling plot for silicon carbide. Experimental and first-principles data from Refs. 62, 69, and 77.

the $\langle 100 \rangle$ dumbbell interstitial: C—C, Si—Si, or C—Si pairs can share either a carbon or a silicon site (C^+—Si$\langle 100 \rangle$, C^+—C$\langle 100 \rangle$, Si^+—C$\langle 100 \rangle$, Si^+—Si$\langle 100 \rangle$; the plus sign indicates the extra atom). There are, furthermore, two different $\langle 110 \rangle$ dumbbell configurations (C^+—C$\langle 110 \rangle$, C^+—Si$\langle 110 \rangle$) which have been investigated. In connection with the aggregation of carbon interstitials Gali et al.[80] have explored a configuration in which two carbon atoms share a silicon site, $(C_2)_{Si}$.

The formation enthalpy for a defect in a neutral charge state can be written as[23,81]

$$\Omega_D = E_D - \frac{1}{2}(n_{Si} + n_C)\mu_{SiC}^{bulk}$$

$$\underbrace{- \frac{1}{2}(n_{Si} - n_C)(\mu_{Si}^{bulk} - \mu_C^{bulk})}_{E_D'}$$

$$- \frac{1}{2}(n_{Si} - n_C)\Delta\mu, \tag{10}$$

where E_D is the total energy of the system in the presence of the defect, n_i is the number of atoms of atom type i, and μ_i^{bulk} is the chemical potential of the *pure* constituent i. The magnitude of $\Delta\mu$ is restricted to be lower or equal than the formation enthalpy ΔH_f. At zero temperature the chemical po-
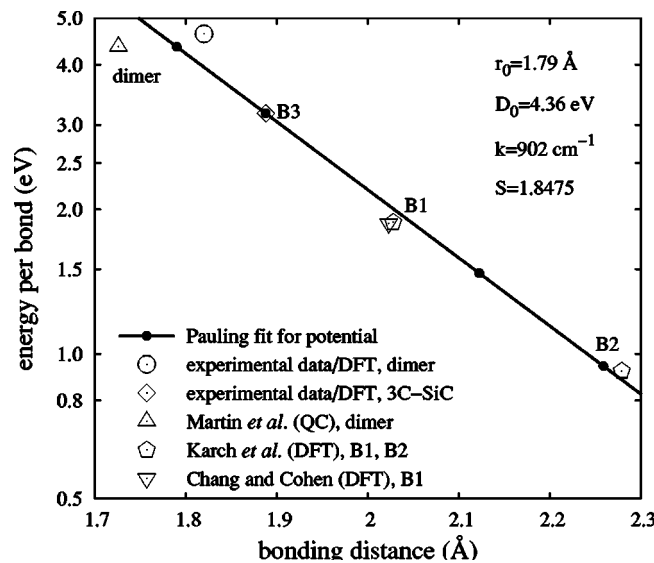
TABLE XIII. Energies and lattice constants for the B1 and B2 structures of silicon carbide. ΔE: energy difference with respect to the B3 structure (eV/atom); a_0: lattice constant (Å).

	DFT		This work		T89	
	ΔE	a_0	ΔE	a_0	ΔE	a_0
B1	0.70–0.72	4.046	1.92	4.244	1.49	4.239
B2	2.66	2.631	3.04	2.668	2.49	2.640
			2.57[a]	2.608[a]		

[a]This value is obtained if the Si—Si cutoff is reduced such that $R+D \leqslant 2.63$ Å.

tentials of the bulk phases are given by the cohesive energies $\mu_{\text{Si}}^{\text{bulk}}=-4.63$ eV/atom, $\mu_{\text{C}}^{\text{bulk}}=-7.374$ eV/atom, and $\mu_{\text{SiC}}^{\text{bulk}}=-12.68$ eV/f.u. with the corresponding formation enthalpy of $\Delta H_f=0.68$ eV/f.u.

In Table XIV point defect formation energies (E_D') calculated with the new potential (silicon parameter set Si-I) are compared to first-principles calculations[78] and the original version of the Tersoff potential (T89).[13] The point defect combinations included in the table preserve the stoichiometry, therefore the defect formation energies are independent of $\Delta\mu$. Note that the formation enthalpies given in Refs. 17, 78, and 79 have been calculated neglecting the effect of the variation of the chemical potential in the vicinity of the defect expressed by term in the second line of Eq. (10). We

have applied this correction to obtain the values in the first and second columns of Table XIV.

The formation enthalpies for vacancies and antisite defects predicted by the new potential are somewhat too low but still in fair agreement with first-principles calculations. The situation regarding the interstitial defects is unclear. The formation enthalpies calculated by Wang *et al.*[79] are consistently higher than those given in Ref. 78. We find good agreement with the former data but quite large deviations from the latter.

In general, the agreement is at least fair as it comes to the energetic ordering. In comparison, the bond-order potential by Gao and Weber[17] which is based on the potential by Dyson and Smith[15] provides a better description of point

TABLE XIV. Formation energies of point defects silicon carbide [E_D' in Eq. (10)] in units of eV. For the new bond-order potential the first and second column show the values obtained with and without overbinding corrections for the C—C interaction, respectively.

	DFT			This work		T89	GW
	Ref. 78	Ref. 79	Ref. 80	w	w/o	Ref. 13	Ref. 17
V_{C}	5.11	4.5	4.2	1.90	1.93		1.39
V_{Si}	8.01	8.2	8.1	4.55	4.55		4.67
$V_{\text{C}}+V_{\text{Si}}$	12.12	12.7		6.99	7.02	7.4	6.48
C_{Si}	4.06	3.8	3.4	2.42	2.19		4.43
Si_{C}	4.46	4.6		2.48	2.36		5.05
$C_{\text{Si}}+Si_{\text{C}}$	8.52	8.4		4.90	4.55	7.2	9.48
C_{TC}	7.78	12.4		12.63	12.68		6.02
C_{TSi}	7.21	10.0		9.38	9.38		5.69
Si_{TC}	4.80	13.3		17.55	17.35		2.60
Si_{TSi}	7.34	13.6		17.30	18.15		5.40
$Si_{\text{TC}}+C_{\text{TSi}}$	12.01	23.3		26.93	26.78	22.6	8.29
$Si_{\text{TSi}}+C_{\text{TC}}$	15.12	26.0		29.93	30.83	23.2	11.42
$C_{\text{TC}}+C_{\text{TSi}}$	0.57	2.4		3.25	3.30	3.0	0.33
C^+—$Si\langle100\rangle$	4.96			8.31	8.24		4.80
C^+—$C\langle100\rangle$	4.53		6.9	4.78	5.12		4.41
Si^+—$C\langle100\rangle$	8.68			14.14	13.37		6.17
Si^+—$Si\langle100\rangle$	7.95			20.90	17.72		4.16
C^+—$C\langle100\rangle$	4.69			9.89	10.64		4.67
C^+—$Si\langle100\rangle$	4.65			4.81	5.12		5.32
$(C_2)_{\text{Si}}$			6.4	4.70	5.03		

defect properties in 3C—SiC, but since the pure silicon and carbon structures parameters were modified, it is lacking the transferability our work is aiming for. In particular, it cannot be applied to model the pure phases and it yields an inappropriate description of the elastic properties as shown in Table XII.

VI. CONCLUSIONS AND OUTLOOK

New bond-order potentials for silicon and silicon carbide have been derived, which allow atomic scale computer simulations of processes involving a wide range of different atomic configurations. Elastic, thermal, and point defect properties are well reproduced. The description of higher coordinated structures by the silicon and carbon parameter sets is comparable to the well established Tersoff potential, while elastic, defect, and thermal properties are superior. The de-

scription of elastic properties of silicon carbide by the new potential is improved with respect to the potentials available in literature. Defect properties are only fairly reproduced but the description is comparable to previously published potentials. The new potential enables modeling of processes which involve widely different configurations and transitions among these. In this spirit, it has been recently applied to the modeling of the inert gas condensation of silicon-carbon nanoparticles, representative for a transition from the molecular to the bulk regime.

*Electronic address: erhart@mm.tu-darmstadt.de

[1] *Silicon Carbide Ceramics 1, Fundamental and Solid Reaction*, edited by S. Sōmiya and Y. Inomata (Elsevier, Amsterdam, 1991).

[2] K. Liethschmidt, in *Ullmann's Encyclopedia of Industrial Chemistry* (VCH, Weinheim, 1993), Vol. A23, p. 749.

[3] M. A. Capano and R. J. Trew, MRS Bull. **22**, 19 (1997).

[4] G. Pensl and R. Helbig, Festkoerperprobleme **30**, 133 (1990).

[5] R. Vaßen, A. Kaiser, and D. Stöver, J. Nucl. Mater. **233–237**, 708 (1996).

[6] S. Sharafat, C. P. C. Wong, and E. E. Reis, Fusion Technol. **19**, 901 (1991).

[7] F. H. Stillinger and T. A. Weber, Phys. Rev. B **31**, 5262 (1985).

[8] J. Tersoff, Phys. Rev. B **37**, 6991 (1988).

[9] J. F. Justo, M. Z. Bazant, E. Kaxiras, V. V. Bulatov, and S. Yip, Phys. Rev. B **58**, 2539 (1998).

[10] M. I. Baskes, Mater. Chem. Phys. **50**, 152 (1997).

[11] D. W. Brenner, Phys. Rev. B **42**, 9458 (1990).

[12] K. Albe, K. Nordlund, and R. S. Averback, Phys. Rev. B **65**, 195124 (2002).

[13] J. Tersoff, Phys. Rev. B **39**, 5566 (1989).

[14] K. Beardmore and R. Smith, Philos. Mag. A **74**, 1439 (1996).

[15] A. J. Dyson and P. V. Smith, Surf. Sci. **355**, 140 (1996).

[16] A. Dyson and P. Smith, Mol. Phys. **96**, 1491 (1999).

[17] F. Gao and W. J. Weber, Nucl. Instrum. Methods Phys. Res. B **191**, 504 (2002).

[18] R. Devanathan, T. Diaz de la Rubia, and W. J. Weber, J. Nucl. Mater. **253**, 47 (1998).

[19] F. Shimojo, I. Ebbsjö, R. K. Kalia, A. Nakano, J. P. Rino, and P. Vashishta, Phys. Rev. Lett. **84**, 3338 (2000).

[20] A. Chatterjee, R. Kalia, A. Nakano, A. Omeltchenko, K. Tsuruta, P. Vashishta, C.-K. Loong, M. Winterer, and S. Klein, Appl. Phys. Lett. **77**, 1132 (2000).

[21] P. Erhart and K. Albe, Appl. Surf. Sci. **226**, 12 (2004).

[22] K. Albe, K. Nordlund, J. Nord, and A. Kuronen, Phys. Rev. B **66**, 035205 (2002).

[23] J. Nord, K. Albe, P. Erhart, and K. Nordlund, J. Phys.: Condens.

Matter **15**, 5649 (2003).

[24] G. C. Abell, Phys. Rev. B **31**, 6184 (1985).

[25] A. P. Horsfield, A. M. Bratkovsky, M. Fearn, D. G. Pettifor, and M. Aoki, Phys. Rev. B **53**, 12 694 (1996).

[26] D. W. Brenner, Phys. Rev. Lett. **63**, 1022 (1989).

[27] P. Erhart and K. Albe (unpublished).

[28] J. Tersoff, Phys. Rev. B **38**, 9902 (1988).

[29] K. P. Huber and G. Herzberg, *Constants of Diatomic Molecules* (Van Nostrand, New York, 1979).

[30] H. Balamane, T. Halicioglu, and W. A. Tiller, Phys. Rev. B **46**, 2250 (1992).

[31] L. Kleinman, Phys. Rev. **128**, 2614 (1962).

[32] C. S. G. Cousins, J. Phys. C **11**, 4867 (1978).

[33] O. H. Nielsen and R. M. Martin, Phys. Rev. B **32**, 3780 (1985).

[34] M. Z. Bazant, E. Kaxiras, and J. F. Justo, Phys. Rev. B **56**, 8542 (1997).

[35] T. J. Lenosky, B. Sadigh, E. Alonso, V. V. Bulatov, T. Diaz de la Rubia, J. Kim, A. F. Voter, and J. D. Kress, Modell. Simul. Mater. Sci. Eng. **8**, 825 (2000).

[36] *Properties of Silicon*, Emis Datareviews Series No. 4, edited by G. L. Harris (INSPEC, London, 1988).

[37] O. H. Nielsen and R. M. Martin, Phys. Rev. B **32**, 3792 (1985).

[38] T. J. Lenosky, J. D. Kress, I. Kwon, A. F. Voter, B. Edwards, D. F. Yang, S. Yang, and J. B. Adams, Phys. Rev. B **55**, 1528 (1997).

[39] J. Crain, S. J. Clark, G. J. Ackland, M. C. Payne, V. Milman, P. D. Hatton, and B. J. Reid, Phys. Rev. B **49**, 5329 (1994).

[40] J. Crain, G. J. Ackland, and S. J. Clark, Rep. Prog. Phys. **58**, 705 (1995).

[41] R. J. Needs and A. Mujica, Phys. Rev. B **51**, 9652 (1995).

[42] M. T. Yin and M. L. Cohen, Phys. Rev. B **26**, 3259 (1982).

[43] M. T. Yin and M. L. Cohen, Phys. Rev. B **29**, 6996 (1984).

[44] *Numerical Data and Functional Relationships in Science and Technology*, edited by H. Ullmeier, Landolt-Börnstein New Series, Group III, Vol. 29, Pt. A (Springer, Heidelberg, 1991).

[45] F. Ercolessi, O. Tomagnini, S. Iarlori, and E. Tosatti, in *Nanosources and Manipulation of Atoms Under High Fields and Tem-*

peratures: Applications, edited by V. T. Binh (Kluwer, Amsterdam, 1993), pp. 185–205.

[46] S. J. Cook and P. Clancy, Phys. Rev. B **47**, 7686 (1993).

[47] H. J. C. Berendsen, J. P. M. Postma, W. F. Gunsteren, A. D. Nola, and J. R. Haak, J. Chem. Phys. **81**, 3684 (1984).

[48] P. Erhart and K. Albe (unpublished).

[49] I. Štich, R. Car, and M. Parrinello, Phys. Rev. B **44**, 4262 (1991).

[50] M. Ishimaru, K. Yoshida, and T. Motooka, Phys. Rev. B **53**, 7176 (1996).

[51] L. Colombo, Annu. Rev. Mater. Sci. **32**, 271 (2002).

[52] *Numerical Data and Functional Relationships in Science and Technology*, edited by H. Ullmeier, Landolt-Börnstein New Series, Group III, Vol. 41, Pt. A2A (Springer, Heidelberg, 2002).

[53] M. J. Puska, S. Pöykkö, M. Pesola, and R. M. Nieminen, Phys. Rev. B **58**, 1318 (1998).

[54] S. Goedecker, T. Deutsch, and L. Billard, Phys. Rev. Lett. **88**, 235501 (2002).

[55] J. Tersoff, Phys. Rev. Lett. **61**, 2879 (1988).

[56] J. Furthmüller, J. Hafner, and G. Kresse, Phys. Rev. B **50**, 15 606 (1994).

[57] S. Q. Wang and H. Q. Ye, J. Phys.: Condens. Matter **15**, 5307 (2003).

[58] R. Q. Hood, P. R. C. Kent, R. J. Needs, and P. R. Briddon, Phys. Rev. Lett. **91**, 076403 (2003).

[59] J. Bernholc, A. Antonelli, T. M. Del Sole, Y. Bar-Yam, and S. T. Pantelides, Phys. Rev. Lett. **61**, 2689 (1988).

[60] K. Karch, F. Bechstedt, P. Pavone, and D. Strauch, Phys. Rev. B **53**, 13 400 (1996).

[61] C. H. Park, B.-H. Cheong, K.-H. Lee, and K. J. Chang, Phys. Rev. B **49**, 4485 (1994).

[62] J. M. L. Martin, J. P. Francois, and R. Gijbels, J. Chem. Phys. **92**, 6655 (1990).

[63] P. F. Bernath, S. A. Rogers, L. C. O'Brien, C. R. Brazier, and A. D. McLean, Phys. Rev. Lett. **60**, 197 (1988).

[64] C. M. Rohlfing and R. L. Martin, J. Phys. Chem. **90**, 2043 (1986).

[65] *Numerical Data and Functional Relationships in Science and Technology*, edited by H. Ullmeier, Landolt-Börnstein New Series, Group III, Vol. 41, Pt. A1A (Springer, Heidelberg, 2001).

[66] W. R. L. Lambrecht, B. Segall, M. Methfessel, and M. van Schilfgaarde, Phys. Rev. B **44**, 3685 (1991).

[67] M. Prikhodko, M. Miao, and W. R. L. Lambrecht, Phys. Rev. B **66**, 125201 (2002).

[68] C.-Z. Wang, R. Yu, and H. Krakauer, Phys. Rev. B **53**, 5430 (1996).

[69] K. Karch, P. Pavone, W. Windl, O. Schütt, and D. Strauch, Phys. Rev. B **50**, 17 054 (1994).

[70] M. Tang and S. Yip, Phys. Rev. B **52**, 15 150 (1995).

[71] T. Halicioglu, Phys. Rev. B **51**, 7217 (1995).

[72] J. Tersoff, Phys. Rev. Lett. **64**, 1757 (1990).

[73] J. Tersoff, Phys. Rev. B **49**, 16 349 (1994).

[74] M. Yoshida, A. Onodera, M. Ueno, K. Takemura, and O. Shimomura, Phys. Rev. B **48**, 10 587 (1993).

[75] T. Sekine and T. Kobayashi, Phys. Rev. B **55**, 8034 (1997).

[76] M. Catti, Phys. Rev. Lett. **87**, 035504 (2001).

[77] K. J. Chang and M. L. Cohen, Phys. Rev. B **35**, 8196 (1987).

[78] F. Gao, E. J. Bylaska, W. J. Weber, and R. Corrales, Phys. Rev. B **64**, 245208 (2001).

[79] C. Wang, J. Bernholc, and R. F. Davis, Phys. Rev. B **38**, 12 752 (1988).

[80] A. Gali, P. Deák, P. Ordejón, N. T. Son, E. Janzén, and W. J. Choyke, Phys. Rev. B **68**, 125201 (2003).

[81] G.-X. Qian, R. M. Martin, and D. J. Chadi, Phys. Rev. B **38**, 7649 (1988).

[82] M. Posselt (private communication).